Additively manufactured Hastelloy-X: effect of post-process heat treatment on microstructure and mechanical properties

Muztahid Muhammad[1,2], Reza Ghiaasiaan[1,2,] Paul R. Gradl[3], Andre Schobel[4], Donald Godfrey[5], Shuai Shao[1,2], Nima Shamsaei[1,2*]

[1]National Center for Additive Manufacturing Excellence (NCAME), Auburn University, Auburn, AL 36849, USA
[2]Department of Mechanical Engineering, Auburn University, Auburn, AL 36849, USA
[3]NASA Marshall Space Flight Center, Propulsion Department, Huntsville, AL 35812, USA
[4]SLM Solutions Group AG, Lübeck, Germany
[5]SLM Solutions NA, Inc. Wixom, MI 48393, USA

*Corresponding author:
shamsaei@auburn.edu
Phone: (334) 844-4839

Abstract

In this study, the effect of post-process heat treatment on the microstructure and mechanical properties of Hastelloy-X superalloy fabricated via two different additive manufacturing technologies, namely, laser beam powder bed fusion (LB-PBF) and laser powder directed energy deposition (LP-DED), is investigated. Microstructure was examined using scanning electron microscopy (SEM) and electron backscattered diffraction (EBSD) analysis, while mechanical properties were evaluated by macro-hardness testing using the Rockwell B method. Microstructure of the alloys was studied thoroughly after several heat treatments that involve stress-relieving (at 1066°C for 1.5 hours), hot isostatic pressing (HIP at 1163°C for 3 hours under 103 MPa pressure), and/or solution treatment (at 1177°C for 3 hours). The results revealed that, for both LB-PBF and LP-DED Hastelloy-X, the post-process heat treatments resulted in uniform grain structure as well as partial dissolution of carbides, although they have different grain sizes.

Keywords: Additive manufacturing, Hastelloy-X, microstructure, grain size, macro-hardness.

Introduction

Due to Hastelloy X's ability to retain high strength at elevated temperatures even in highly corrosive environments, it is extensively used to fabricate parts with a complex structure typically used in power generation gas turbines and aerospace industries [1,2]. However, as it is quite challenging to machine these Ni-base parts, additive manufacturing (AM)—having the capability to fabricate finished complex parts— can be a suitable alternative manufacturing process for this alloy. Among different AM methods, laser beam powder bed fusion (LB-PBF) and laser powder directed energy deposition (LP-DED) are two well-known and extensively used techniques. In the LB-PBF process,

powders are spread uniformly over a build platform, and a heat source melts the powders together to fabricate parts [3]. In the LP-DED technique, powder particles are injected for deposition and melted to fabricate parts [4].

In spite of AM techniques providing several advantages over the traditional manufacturing methods, the mechanical properties of AM parts may differ from those of the conventionally fabricated parts. For instance, the microstructure of AM parts often differs from the conventionally fabricated parts due to the unique thermal history during the manufacturing process leading to the process-induced volumetric defects and residual stresses, which in turn may impact the mechanical properties of the AM components. The larger variation in characteristic thermal history among different AM technologies also exacerbates this. Hence, utilizing the same heat treatment procedures proposed in the literature for the wrought counterparts on the AM components may not necessarily result in similar mechanical performance [5]. Therefore, there is a knowledge gap for thorough verification of the applicability of the conventional heat treatment processes proposed for the wrought component on the AM materials.

Hastelloy-X is a primarily solid solution and partially carbide strengthened Ni-base superalloy [6,7]. The absence of Nb in Hastelloy X, a potential δ and Laves phase former, may potentially give it better mechanical properties in as-fabricated conditions compared to other alloys with Nb. Although microstructure and mechanical properties of Hastelloy X has been investigated in both wrought [2,6–8] and various AM conditions [9–14], the effect of multiple-step heat treatments, which are often necessary for AM parts, on both microstructure and mechanical properties of AM Hastelloy-X fabricated by different AM processes and their comparison is still lacking. In this paper, the effect of multiple-step heat treatments on the microstructure and mechanical properties of LB-PBF and LP-DED Hastelloy-X has been thoroughly investigated and compared.

Experimental Procedure

Cylindrical bars of Hastelloy-X with 14 mm diameter and 90 mm height were fabricated using both LB-PBF and LP-DED techniques. The LB-PBF Hastelloy-X bars were fabricated by SLM280 2.0 machine using a pre-heated build platform (recommended by SLM solutions) at 200ºC. **Table 1** and **Table 2** list the process parameters and chemical composition of powders used in this study for the fabrication of test samples by the LB-PBF and LP-DED process, respectively. The LP-DED bars were fabricated by the RPM Innovations (RPMI), while the LB-PBF bars were produced by SLM Solutions. 5-mm thick test coupons were cut for microstructural analysis. The test coupons were heat treated using an electric furnace with a heating rate of 5ºC/minute.

Detailed descriptions of the multiple-step heat treatment processes used in this study, along with the designations used hereafter in this article to identify each test sample, are listed in **Table 3**, which are further schematically shown in **Figure 1**. The heat treatment process could consist of three consecutive steps [15–17]. As Step 1, a stress-relieving (SR) at 1066°C for 1.5 hr followed by air cooling to ambient temperature, and as Step 2, a hot isostatic pressing (HIP) process at 1163°C under 103 MPa isostatic pressure for 3

hr [6,18] followed by argon quench to room temperature, and finally as Step 3, a solution treatment at 1177°C followed by argon quench or water quench [6,8,18] to room temperature.

Microstructural coupons were mounted, ground, and polished in the plane perpendicular to the build direction according to ASTM-E3 [19]. A Zeiss Crossbeam 550 scanning electron microscope (SEM) equipped with energy dispersive spectroscopy (EDS) and Electron backscatter diffraction (EBSD) detectors were used for microstructural analyses. An electron channeling contrast imaging (ECCI) technique [20] was used to obtain the backscattered secondary electron (BSE) micrographs. It should be noted that EBSD analysis using a step size of 0.43 μm was conducted for grain size measurement; therefore, grains smaller than 0.43 μm were excluded from the analysis.

A Leco LCR500 Rockwell-type hardness tester was used to measure the macro-hardness of the test samples in various heat treatment conditions by a Rockwell B indenter using 100 kgf load according to ASTM E18 standard [21,22]. It should be noted that each mean value reported in this study was calculated over at least 5 hardness readings.

Table 1. Process parameters used in this study for fabrication of the LB-PBF and LP-DED Hastelloy-X test samples.

Process	Power (W)	Layer thickness (μm)	Scan speed (mm/sec)	Travel speed (mm/min)	Hatch distance (μm)	Powder feed rate (g/min)
LB-PBF	200	30	1000	-	100	
LP-DED	1070	381	-	1016	-	16

Table 2. Chemical composition of powders used for fabrication of LB-PBF and LP-DED Hastelloy-X test samples in this study.

Wt.%	LB-PBF Hastelloy-X	LP-DED Hastelloy-X
Ni	Balance	Balance
Cr	21.95	21.68
C	0.05	0.10
Co	1.58	1.53
Fe	18.63	18.97
Mn	0.01	0.01
Mo	8.78	8.73
P	-	<0.005
S	-	<0.001
Si	0.25	0.08
W	0.58	0.60

.

Table 3. Heat treatments (with designations) conducted on LB-PBF and LP-DED Hastelloy-X in this study.

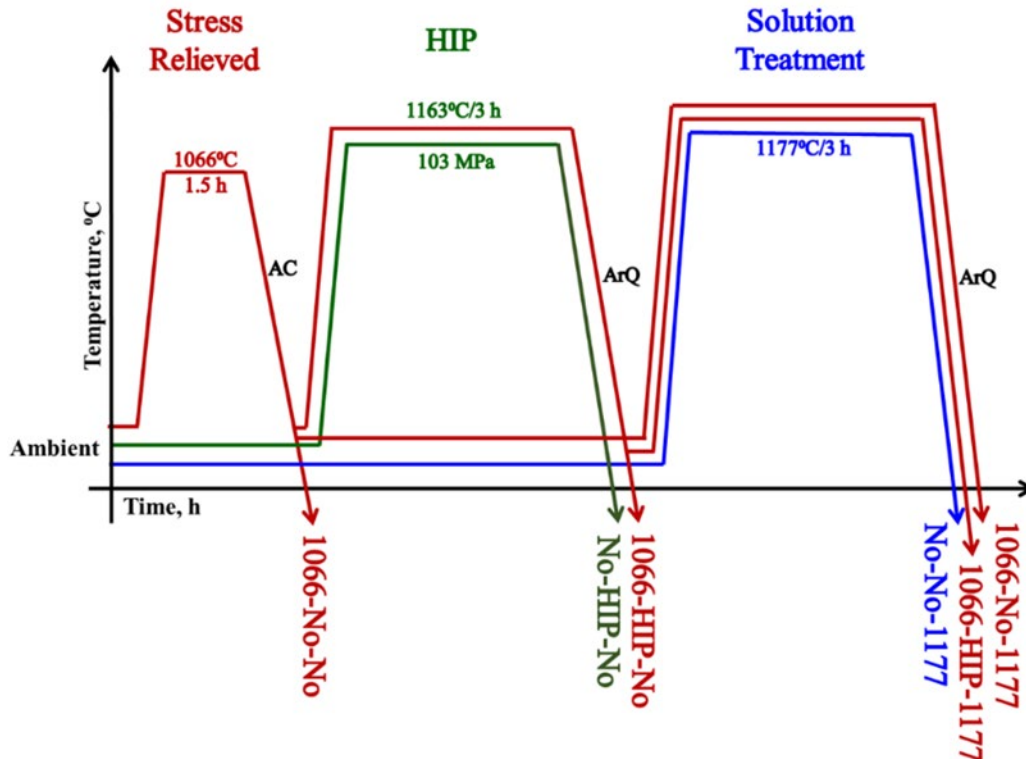| Heat treatment	Step 1 (Stress-relieving)			Step 2 (HIP)			Step 3 (Soltutionizing)			Designation
	Temp. (ºC)	Time (hr)	Cooling Media	Temp. (ºC)	Time (hr)	Pressure (MPa)	Temp. (ºC)	Time (hr)	Cooling Media	
As-built		No			No			No		NHT (Non-heat treated)
Stress-releived	1066ºC	1.5 h	Argon		No			No		1066-No-No
HIP		No		1163ºC	3 h	100 MPa		No		No-HIP-No
Solutionized		No			No		1177ºC	3 h	Argon	No-No-1177
Stress-releived + HIP	1066ºC	1.5 h	Argon	1163ºC	3 h	100 MPa		No		1066-HIP-No
Stress-releived + Solutionized	1066ºC	1.5 h	Argon		No		1177ºC	3 h	Argon	1066-No-1177
Stress-releived + HIP + Solutionized	1066ºC	1.5 h	Argon	1163ºC	3 h	103 MPa	1177ºC	3 h	Argon	1066-HIP-1177

Figure 1. Schedules of heat treatment conducted on both LB-PBF and LP-DED Hastelloy-X alloy in this study.

Results and Discussion

Inverse pole figure (IPF) maps obtained from EBSD analysis in the plane perpendicular to the build direction for LB-PBF and LP-DED Hastelloy-X test samples in various heat treatments used in this study are shown in **Figure 2**. As shown **Figure 2**, the average grain sizes of the LB-PBF Hastelloy X alloy in various heat treatment conditions, ranging from 46 μm for the non-heat treated (NHT or as-built) sample to 38 μm for the fully heat treated one (**Figures 2**(a)-(g)), are smaller than those of the LP-DED samples, ranging from 53 μm for No-HIP-No to 65 μm for the fully heat treated conditions (see **Figures 2**(i)-(n)). The differences in grain size between LB-PBF and LP-DED Hastelloy-X can be attributed to differences in layer height (see **Table 1** and **Table 2**) of LB-PBF and LP-DED processes as well as possible differences in the chemical composition of their powders. The difference in chemistry may lead to more or less carbides, which are effective grain boundary pinners. It should be noted that the finer grain sizes observed in the LB-PBF alloy may have a slight improving effect on the strength of the alloy as compared with the LP-DED samples, according to the Hall-Petch relationship [23]. Furthermore, it is shown in **Figure 3** that the further multiple steps of post heat treatments have a homogenization effect on the grain size distribution of both the LB-PBF and LP-DED samples.

It should be noted that the multiple-step heat treatments resulted in a decrease in average grain sizes of the LB-PBF alloy compared to the NHT condition (see **Figure 2**), while in the case of the LP-DED samples, the subsequent heat treatment has a minimal

effect on the average grain size of the alloy. This can be further shown in **Figure 4**, where the BSE micrographs obtained by ECCI technique for both LB-PBF and LP-DED alloys are shown and compared in two magnifications for all the heat treatment conditions investigated in this study. As shown in low magnified BSE images (c) to (g), the subsequent heat treatments above 1066°C (i.e., stress relieving) have successfully removed the prior dendritic microstructure observed in the NHT condition of the LB-PBF Hastelloy X alloy (see in (a)). However, this is not the case for the LP-DED alloy, and it seems that the subsequent heat treatments could only partially dissolve the inter-dendritic regions, as shown in **Figures 4**(i) to (vii).
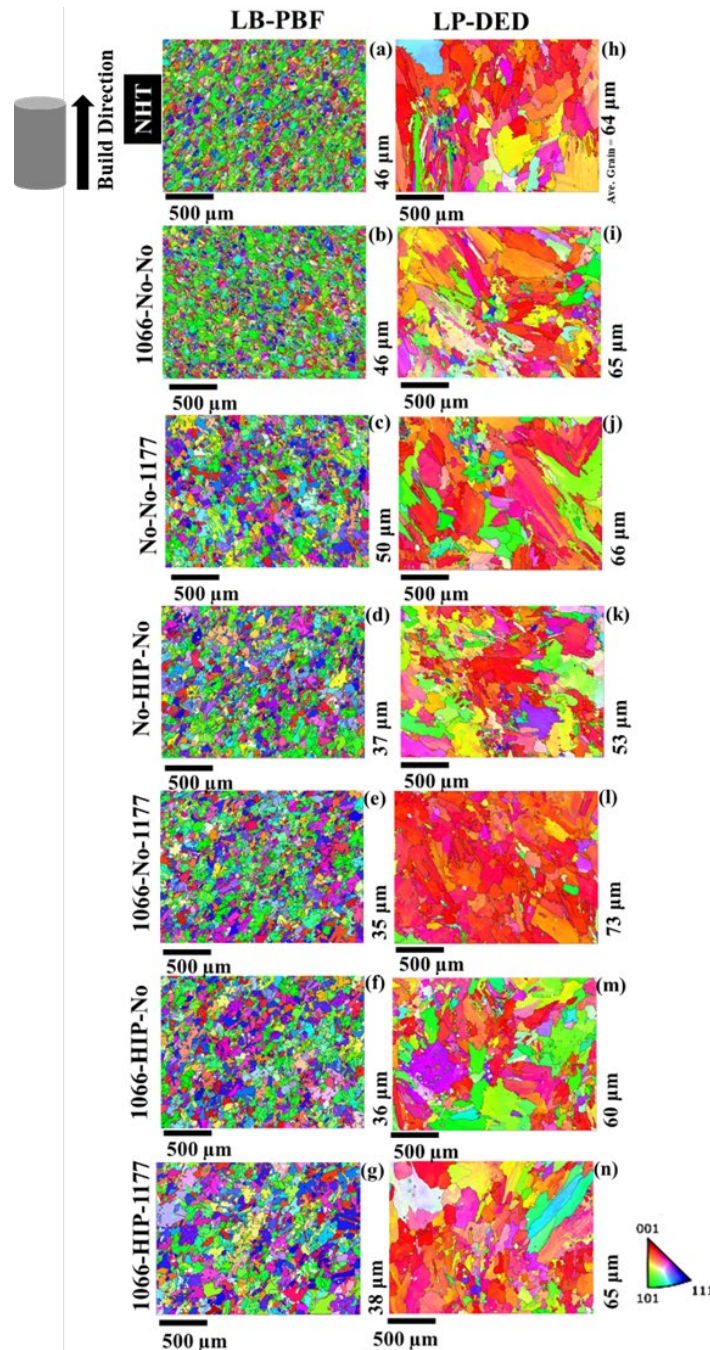
Figure 2. Inverse pole figure (IPF) maps obtained by EBSD analysis on the plane perpendicular to the build direction in (a) to (g) for the LB-PBF Hastelloy-X alloy and in (h) to (n) for the LP-DED samples in various heat treatment conditions investigated in this study.

These different effects of heat treatment on the LB-PBF and LP-DED Hastelloy X microstructure could partly be attributed to the differences in the chemical composition, especially the carbon content of powder used for the LB-PBF and LP-DED processes. Specially, the LB-PBF powder batch may have lower carbon content, which can explain the lower fraction of carbides and more recrystallization/growth seen in the heat treated LB-PBF microstructure. Further, as shown in high magnification BSE images, some phases were formed at grain boundaries of both the LB-PBF and LP-DED alloys, as shown in **Figures 4**(h)–(o) and (viii)–(xiv), respectively. For the LB-PBF samples, such phases may be the Cr-rich ($M_{23}C_6$) and Mo-rich (M_6C) carbides [2,9,24]. However, for the LP-DED samples, these phases could be identified as the Laves phases, according to Ref [14].
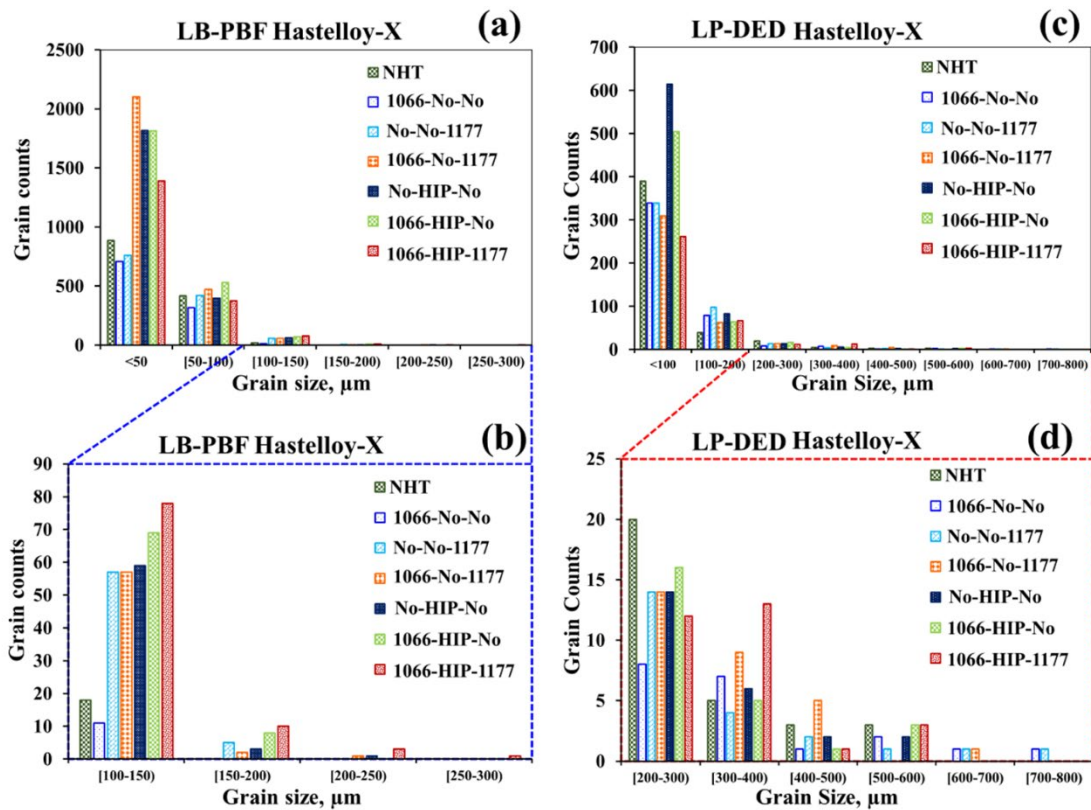

Figure 3. Typical comparative column graph for the grain size distributions of LB-PBF and LP-DED Hastelloy-X alloys in various heat treatment conditions investigated in this study in (a)-(b) and (c)-(d), respectively.

For parts fabricated using AM technology, it is recommended to conduct stress relief to remove residual stresses [25]. It can be seen from the IPF maps (see **Figures 2**(b) and (i) and **Figure 3**) that conducting stress-relieving at 1066ºC (i.e., 1066-No-No) on both LB-PBF and LP-DED Hastelloy-X partially homogenized the grains. It has been

reported in the literature that exposure to high temperatures (1066ºC for 1.5 hours) may cause partial homogenization [25,26]. However, after stress relief, the average grain size is almost unchanged for 1066-No-No LB-PBF and LP-DED Hastelloy-X alloy compared to NHT conditions.
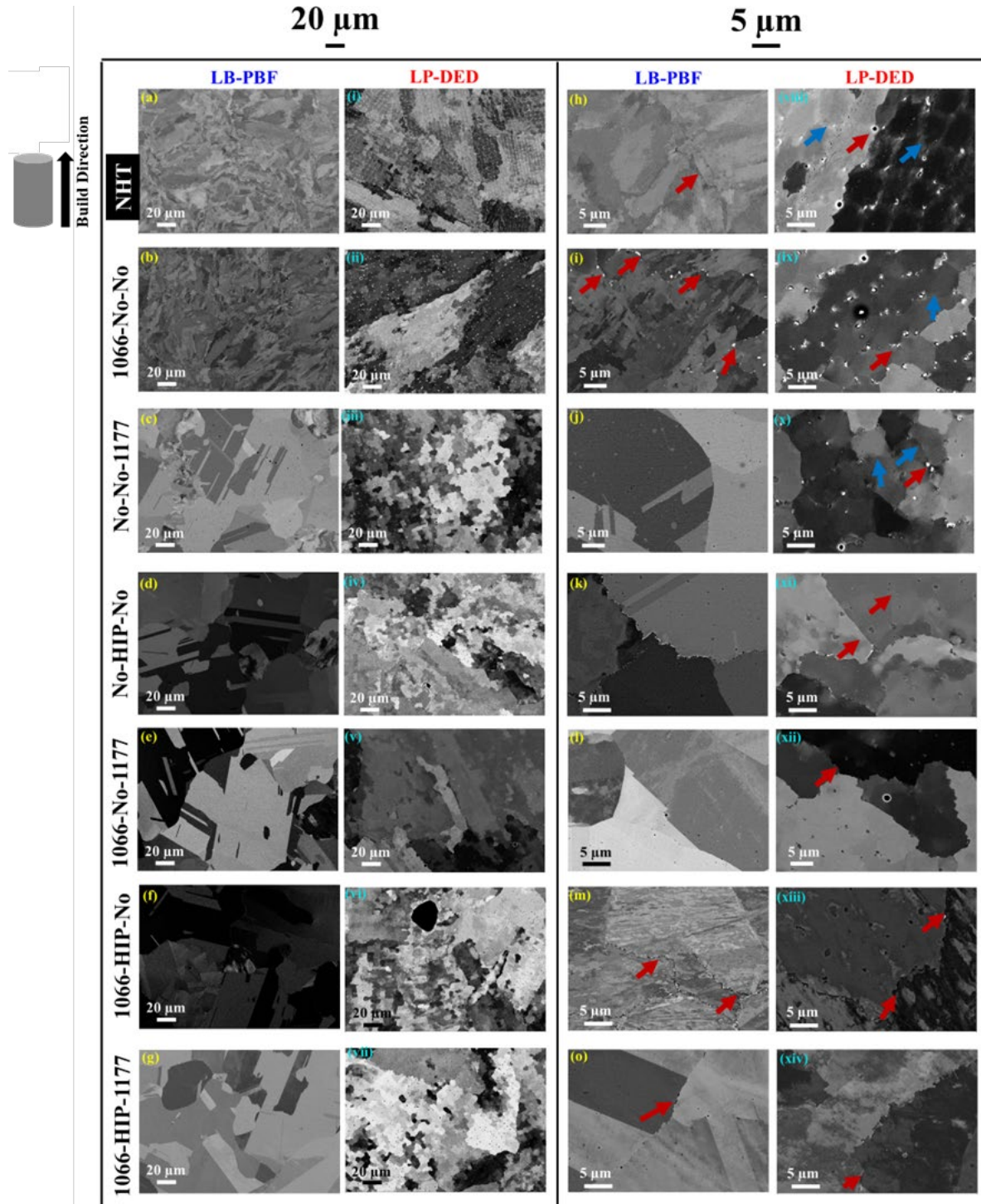

Figure 4. Typical BSE micrographs in two magnifications obtained in the plane perpendicular to build direction for the LB-PBF Hastelloy-X in (a) to (o) as well as the

LP-DED Hastelloy-X in (i) to (xiv) in various heat-treated conditions. Red arrows are pointing to the carbides, and blue arrows are pointing to the micro-segregations.

The comparative column graph of the macro-hardness measurements obtained by the Rockwell B (HRB) method is presented in **Figure 5** for both the LB-PBF and LP-DED alloys in various heat treatment conditions. As shown, the HRB macro-hardness values of the LB-PBF samples are significantly higher than those of the LP-DED counterparts for all heat treatment conditions that do not include HIP. This could partly be ascribed to the strengthening effect of grain sizes, according to the Hall-Petch relationship [23]. It should be noted that upon the first step low-temperature stress-relieving at 1066°C, the hardness of the LB-PBF samples have not significantly changed, which could be ascribed to the strengthening effect [9] of remnants of the inter-dendritic regions (see **Figure 4**(b)) as compared with the other higher temperature heat treatments (see **Figures 4**(b)–(g)).
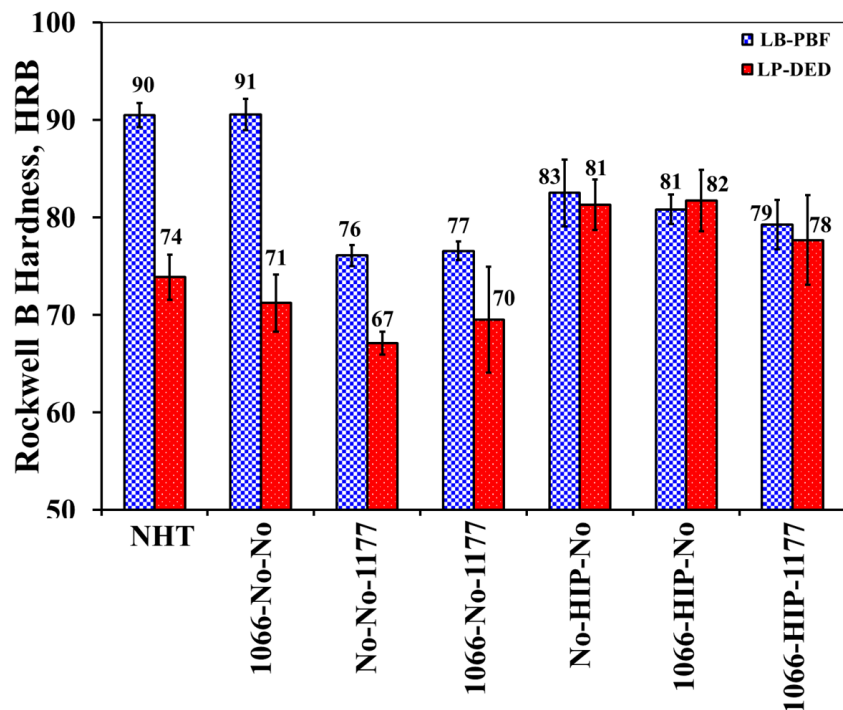

Figure 5. Comparative column graph for the Rockwell B hardness values of LB-PBF and LP-DED Hastelloy-X samples in various heat treatment conditions investigated in this study.

Among different heat treatments of LB-PBF Hastelloy-X, NHT and 1066-No-No exhibit the highest hardness (~90 HRB). The presence of fine grains along with the fine dendritic microstructure might have contributed to the high hardness of LB-PBF Hastelloy-X in NHT condition (see **Figure 4**(h)). After No-No-1177 and 1066-No-1177, grains of LB-PBF Hastelloy-X have been significantly homogenized, and carbides from inter-dendritic regions have been dissolved (see **Figures 4**(j) and (l)). The dissolution of dendritic microstructure might result in the decrease in hardness values of No-No-1177 and 1066-No-1177 LB-PBF Hastelloy-X samples (~15%) compared to NHT and 1066-No-No conditions. On the other hand, although No-HIP-No and 1066-HIP-No heat treatments

homogenized the grains, the formation of carbides along grain boundaries (see **Figures 4**(k) and (m)) increased the indentation force response of LB-PBF Hastelloy-X since carbide strengthen Hastelloy-X. Consequently, No-HIP-No and 1066-HIP-No LB-PBF Hastelloy-X exhibit slightly higher hardness (~6%) compared to 1066-No-No and 1066-No-1177 conditions. The three HIPed conditions did not yield similar hardness values for LB-PBF samples.

Formation of the inter-dendritic region and inter-dendritic carbides (see **Figure 4**(viii)) contributed to the higher strength of NHT LP-DED Hastelloy-X (~74 HRB) compared to 1066-No-No (~71 HRB), No-No-1177 (~67 HRB), and 1066-No-1177 (~70 HRB) LP-DED Hastelloy-X conditions. With partial dissolution inter-dendritic region (see **Figure 4**(ix)), the strength of 1066-No-No LP-DED Hastelloy-X slightly decreased compared to the NHT condition; which resulted in a slight decrease (~4%) in hardness value of the 1066-No-No condition. Dissolution of the inter-dendritic region, as well as partial dissolution of inter-dendritic carbides in No-No-1177 and 1066-No-1177 LP-DED Hastelloy-X (see Figures 4(x) and (xii)), resulted in the lowest hardness values among all other conditions. After No-HIP-No and 1066-HIP-No post-processing conditions, the phases in the prior inter-dendritic regions were well dissolved which may have improved the degree of solid solution and increased their strength (~8% increase in HRB). These resulted in the highest hardness (~81 HRB) of LP-DED Hastelloy-X in No-HIP-No and 1066-HIP-No among all the heat treated LP-DED Hastelloy-X. The three HIPed conditions did not yield similar hardness values for LP-DED samples. It is also interesting to note that both LB-PBF and LP-DED materials had quite comparable hardness values in HIPed conditions.

Conclusions

In this study, the effect of multiple-step heat treatment on microstructure and mechanical properties of the Hastelloy X fabricated using two different AM processes, including LB-PBF and LP-DED are investigated and compared. The test samples underwent multiple combinations of heat treatments such as stress-relieving (SR) at 1066°C for 1.5 hr, followed by hot isostatic pressing (HIP) at 1163°C at103 MPa for 3 hr, and a solution heat treatment at 1177°C for 3 hr. The microstructure as the result of each single- and/or multi-stage heat treatment was characterized. Further, the macro-hardness of the test samples was measured using the Rockwell B (HRB) method. Below is a brief summary of experimental observations from this study:

- The EBSD analysis reveals that the subsequent heat treatments have a homogenization effect on the grain structure of both the LB-PBF and LP-DED materials; however, the latter has shown larger grain sizes in various hat treatments as compared with the former, which could partly be ascribed higher layer height used in the RPM Innovation machine for fabrication of the LP-DED samples as well as possible differences in the chemical composition of powders used in LB-PBF and LP-DED processes.
- The BSE micrographs reveal that the prior dendritic microstructure of the as-deposited LP-DED samples are hardly dissolved upon subsequent heat

treatments. However, for the LB-PBF samples, the prior inter-dendritic regions are almost completely removed upon the subsequent heat treatments except for the single-step stress relieving at 1066°C (1066-No-No).

- The HRB hardness measurements show that the LP-DED samples show lower HRB hardness values than those of the LB-PBF counterparts, which could be attributed to grain size strengthening.
- Upon subsequent heat treatments without HIP, both materials have shown a softening effect. However, the hardness of the LB-PBF samples was significantly higher in NHT and stress-relieved (SR at 1066°C) conditions, as compared with that of solution treated samples at 1177°C, which could be attributed to the strengthening effect of the much finer prior dendritic microstructure.

Acknowledgment

References

[1]   Haynes Internatioal Website, Hastelloy X: Tensile Properties.

[2]   M. Aghaie-Khafri, N. Golarzi, Forming behavior and workability of Hastelloy X superalloy during hot deformation, Mater. Sci. Eng. A. 486 (2008) 641–647.

[3]   S. Bremen, W. Meiners, A. Diatlov, Selective Laser Melting, Laser Tech. J. 9 (2012) 33–38.

[4]   M. Molitch-Hou, Overview of additive manufacturing process, Addit. Manuf. (2018) 1–38.

[5]   P.D. Nezhadfar, R. Shrestha, N. Phan, N. Shamsaei, Fatigue behavior of additively manufactured 17-4 PH stainless steel: Synergistic effects of surface roughness and heat treatment, Int. J. Fatigue. 124 (2019) 188–204.

[6]   G. Marchese, E. Bassini, A. Aversa, M. Lombardi, D. Ugues, P. Fino, S. Biamino, Microstructural Evolution of Post-Processed Hastelloy X Alloy Fabricated by Laser Powder Bed Fusion, Materials (Basel). 12 (2019) 486.

[7]   G.V.P. Reddy, P. Harini, R. Sandhya, K.B.S. Rao, R.K. Paretkar, On dual-slope linear cyclic hardening of Hastelloy X, Mater. Sci. Eng. A. 527 (2010) 3848–3851.

[8]   HASTELLOY ® X ALLOY A nickel-base alloy with an exceptional combination of oxidation resistance, fabricability and high-temperature strength. H-3009A, 1997.

[9]   R. Ghiaasiaan, M. Muhammad, P.R. Gradl, S. Shao, N. Shamsaei, Superior tensile properties of Hastelloy X enabled by additive manufacturing, Mater. Res. Lett. 9 (2021) 308–314.

[10]   G. Marchese, M. Lorusso, S. Parizia, E. Bassini, J.W. Lee, F. Calignano, D. Manfredi, M. Terner, H.U. Hong, D. Ugues, M. Lombardi, S. Biamino, Influence of heat treatments on microstructure evolution and mechanical properties of Inconel 625 processed by laser powder bed fusion, Mater. Sci. Eng. A. 729 (2018) 64–75.

[11] O. Sanchez-Mata, X. Wang, J.A. Muñiz-Lerma, S.E. Atabay, M. Attarian Shandiz, M. Brochu, Dependence of mechanical properties on crystallographic orientation in nickel-based superalloy Hastelloy X fabricated by laser powder bed fusion, J. Alloys Compd. 865 (2021) 158868.

[12] D. Tomus, Y. Tian, P.A. Rometsch, M. Heilmaier, X. Wu, Influence of post heat treatments on anisotropy of mechanical behaviour and microstructure of Hastelloy-X parts produced by selective laser melting, Mater. Sci. Eng. A. 667 (2016) 42–53.

[13] O. Sanchez-Mata, J.A. Muñiz-Lerma, X. Wang, S.E. Atabay, M. Attarian Shandiz, M. Brochu, Microstructure and mechanical properties at room and elevated temperature of crack-free Hastelloy X fabricated by laser powder bed fusion, Mater. Sci. Eng. A. 780 (2020) 139177.

[14] W. Zhang, Y. Zheng, F. Liu, D. Wang, F. Liu, C. Huang, Q. Li, X. Lin, W. Huang, Effect of solution temperature on the microstructure and mechanical properties of Hastelloy X superalloy fabricated by laser directed energy deposition, Mater. Sci. Eng. A. 820 (2021) 141537.

[15] ASTM F3301, Standard for Additive Manufacturing – Post Processing Methods – Standard Specification for Thermal Post-Processing Metal Parts Made Via Powder Bed Fusion, ASTM Stand. (2018) 3.

[16] H. V Atkinson, S. Davies, Fundamental Aspects of Hot Isostatic Pressing: An Overview, Metallurgical and Materials Transactions A 31 (2000) 2981–3000.

[17] Hot Isostatic Pressing (HIP) conditions | GE Additive.

[18] D.A.A. Sadek Tadros, D.G.W. Ritter, C.D. Drews, D. Ryan, Additive Manufacturing of Fuel Injectors, Pittsburgh, PA, and Morgantown, WV (United States), 2017.

[19] A.E.− 11 (Reapproved 2017) Interanational, Standard Guide for Preparation of Metallographic Specimens Standard Guide for Preparation of Metallographic Specimens 1, ASTM Int. 03.01 (2012) 1–12.

[20] S. Zaefferer, N.-N. Elhami, Theory and application of electron channelling contrast imaging under controlled diffraction conditions, Acta Mater. 75 (2014) 20–50.

[21] ASTM Standard E18-20, Standard Test Methods for Rockwell Hardness of Metallic Materials, (2020).

[22] B. Vieille, C. Keller, M. Mokhtari, H. Briatta, T. Breteau, J. Nguejio, F. Barbe, M. Ben Azzouna, E. Baustert, Investigations on the fracture behavior of Inconel 718 superalloys obtained from cast and additive manufacturing processes, Mater. Sci. Eng. A. (2020).

[23] G.E. Dieter, Mechanical Metallurgy, 3rd ed., McGraw-Hill, Boston, MA, MA, 1986.

[24] W.Z. Abuzaid, M.D. Sangid, J.D. Carroll, H. Sehitoglu, J. Lambros, Slip transfer and plastic strain accumulation across grain boundaries in Hastelloy X, J. Mech. Phys. Solids. 60 (2012) 1201–1220.

[25] K. Gruber, R. Dziedzic, B. Kuźnicka, B. Madejski, M. Malicki, Impact of high temperature stress relieving on final properties of Inconel 718 processed by laser powder bed fusion, Mater. Sci. Eng. A. 813 (2021) 141111.

[26] Y. Zhao, K. Li, M. Gargani, W. Xiong, A comparative analysis of Inconel 718 made by additive manufacturing and suction casting: Microstructure evolution in homogenization, Addit. Manuf. 36 (2020) 101404.